Microscopic Analysis and Applications of the $Cu(Sb,Bi)S_2$ High Optical Absorption

C. Tablero

Instituto de Energía Solar, E.T.S.I. de Telecomunicación,
Universidad Politécnica de Madrid,
Ciudad Universitaria s/n, 28040 Madrid, SPAIN.

Abstract

Ternary $Cu(Sb,Bi)S_2$ semiconductors are a group of materials with a wide variety of applications, especially photovoltaic. An analysis of the structural, electronic and optical properties obtained from first-principles is presented. The microscopic justification of the high absorption coefficients is carried out by splitting the optical properties on chemical species contributions according to the symmetry. Focusing on photovoltaic applications, and from first-principles results, the efficiencies for several solar spectrums are obtained as a function of the device thickness. This study indicates the great potential of these materials for photovoltaic and other optical devices.

Keywords: electronic structure, semiconductors, optical absorption, photovoltaics.

I. INTRODUCTION

A great deal of effort to characterize binary semiconductor systems has been made to find new materials with the physical properties appropriate for photovoltaics. These efforts have led to the exploration of more complex ternary and quaternary structures such as $Cu(In,Ga)Se_2$ (CIGS) [1-5] and $Cu_2ZnSn(S,Se)_4$ (CZTSSe) [6-11] type compounds.

The energy band-gaps of the ternary $CuMS_2$ (M=Sb, Bi) compounds fall within the range for a light absorbent material. The experimental $CuSbS_2$ ($CuBiS_2$) band-gap is between 1.38-1.89 eV [12-15] (1.65-1.8 eV [16,17]). In addition to the energy band-gap, a main physical property for photovoltaics is a large absorption in the visible region (1.65

- 3.1 eV). The absorption coefficients of $CuSbS_2$ and $CuBiS_2$ compounds are about twice that of some conventional Cu-based photovoltaic materials [13,18]. In almost all cases they are above 10^5 cm^{-1} in a wide range of the visible region. Other criteria not based on physical properties are that the materials contain non-toxic and earth abundant elements.

A significant part of previous research into $CuMS_2$ semiconductors has focused on outlining the synthetic method necessary to produce it. Thin films of $CuSbS_2$ have been deposited using several techniques: spray pyrolysis [19], direct evaporation [20] and chemical bath deposition followed by annealing [21,22]. Analyses of the thermodynamic stability indicate that these materials are stable and comparable with other metal sulphide materials [18, 23].

The study of the electronic and structural properties of ternary copper sulfide materials is complex because there are at least three symmetrically non-equivalent atoms. But a greater understanding of these properties is required because they mainly determine the optical properties, which are crucial for the photovoltaic behavior. The final objective of this study is the microscopic understanding of the high absorption of these materials. To do so, we obtain the optical properties from the electronic and structural properties using first-principles. For a better understanding, it will be split into different components. Finally, the potential of these materials as light absorbers in solar cells will be analyzed using the theoretical optical properties for obtaining the efficiencies.

II. CALCULATIONS

The electronic and optical properties have been obtained using first-principles based on the density functional theory (DFT) [24,25]. In traditional DFT the interactions

are treated using a mean field approach. It is not appropriate for describing the correlation effects suitably. Because of spurious electron self-interactions, it leads to an underestimation of the band-gap, an overestimation of the band-width, an underestimation of bond-length of weakly bound molecules and solids, and an overestimation of the binding energy, etc. Methods such as DFT+U and hybrid DFT incorporate a U factor or a fraction of exact exchange in order to avoid the self-interaction problem partially. We will use the DFT+U method [26-27]. The U value depends on the choice of the orbitals on which the correction is applied, on the way the orbital occupations are computed, and on the DFT+U implementation chosen [27-30]. In this work we applied the orbital-dependent one-electron potential using the DFT+U formalism described in references [27-28].

For the exchange-correlation potential, we use the generalized gradient approximation (GGA) from Perdew, Burke and Ernzerhof [31]. The standard Troullier–Martins [32] pseudopotentials are adopted and expressed in the Kleinman–Bylander [33] form. The valence wave functions are expanded into a numerically localized pseudoatomic orbital basis set [34]. In all results presented we use periodic boundary conditions, spin polarization, double-zeta with polarization localized basis sets, and the *Pnma* orthorhombic structure with 116 special k-points in the irreducible Brillouin zone.

Furthermore, in order to obtain the optical properties, we have calculated the momentum ($\mathbf{p} = i(m/\hbar)[H, \mathbf{r}]$) matrix elements $p_{\mu\lambda}$ and the complex dielectric function

$$e_2(E) \sim \frac{1}{E^2} \sum_{\mu<\lambda} \int d\vec{k}\ [f_{\mu,\vec{k}} - f_{\lambda,\vec{k}}] |p_{\mu\lambda}|^2\, \delta(E_{\lambda,\vec{k}} - E_{\mu,\vec{k}} - E) \qquad (1)$$

Other optical properties are obtained via the Kramers-Kronig relationship. Here $E_{\mu,\vec{k}}$ and $f_{\mu,\vec{k}}$ are the single-particle energies and occupations of the μ band at $\vec{k}$ points in the

Brillouin zone. Both, the local and non-local parts of the pseudopotentials have been considered in the calculation of the momentum matrix elements.

III. RESULTS AND DISSCUSION

1. Structure and band structure

$CuMS_2$ (M=Sb, Bi) compounds crystallize into orthorhombic structure *Pnma* (space group 62). In this structure there are two non-equivalent S atoms symbolized by S_1 and S_2 with equal proportions. Therefore, according to this classification, the chemical equation is $CuM(S_1)(S_2)$. The distribution of the first shells of the nearest neighbors around M, Cu, S_1 and S_2 atoms are S_1+2S_2, $2S_1+2S_2$, M+2Cu and 2M+2Cu respectively. The Bi (or Sb) form trigonal pyramids linked to three S atoms (S_1+2S_2) and the Cu have a tetrahedral environment surrounded by $2S_1+2S_2$. Sb in the chalcostibite ($CuSbS_2$) structure has the experimental lattice parameters (a,b,c)=(6.0160, 3.7968, 14.4990) Å and $\alpha=\beta=\gamma=90^0$, and Bi in the emplectite ($CuBiS_2$) structure (a,b,c)=(6.1413, 3.9191, 14.524) Å and $\alpha=\beta=\gamma=90^0$ [35].

The experimental band-gaps reported in the literature for $CuSbS_2$ are between 1.38-1.89 eV: 1.38 eV [12], 1.44 eV [13], 1.52 eV [14], 1.89 eV [15]. The theoretical energy band-gaps using the standard PBE exchange-correlation functional in the literature are 0.90 eV [23], 0.79 eV [18]. With more sophisticated methods the band-gaps reported are 1.56 (HSE06+GW) [13], 1.69 eV (HSE06) [23], and 1.72 (HSE) [18]. For $CuBiS_2$, the experimental band-gaps are between 1.65 eV [38] and 1.8 eV [39]. The theoretical band-gaps using the PBE exchange-correlation functional are 0.36 eV [23] and 0.57 eV [18]. The energy band-gaps obtained with more sophisticated methods are 1.26 (GW+HSE06) [13], 1.55 eV (HSE06) [23], 1.58 eV (HSE06) [18]. For both $CuSbS_2$ and $CuBiS_2$ the energy band-gaps are indirect. Nevertheless, the difference between the lowest energy direct

and indirect band-gaps is ~ 0.1 eV. Therefore a strong direct optical absorption is expected [18, 23].

In our study we have used several GGA+U schemes in order to apply the orbital-dependent one-electron potential: U=5 eV and U=10 eV for the d(Cu) states, and U=5 eV and U=10 eV for all d(Cu), p(S) and p(Sb) states (U_a=5 eV and U_a=10 eV respectively). The energy band-gap obtained with U=0, U=5 eV, U_a=5 eV, and U_a=10 eV are 0.81, 1.04, 1.19, and 1.47 eV for M=Sb, and 0.87, 1.11, 1.25, and 1.57 eV for M=Bi respectively. We found that U_a=5 eV and U_a=10 eV schemes gave energy band gap values closer to the experimental, whereas the other U schemes tend towards energy band-gap underestimation. The energy-band diagram along high symmetry lines in the BZ using GGA+U with U_a=5 eV is shown in Figure 1. The quantitative differences are mainly in the energy band-gap. However, the qualitative results of other properties are similar to the GGA results (U=0). For this reason we will show the comparison between different GGA+U schemes despite of the quantitative energy band-gap differences.

The DFT+U corrects the spurious self-interaction for the orbital subspace (OS) where it is applied, while the remaining ones are still affected by the self-interaction error [27]. The effect on a band of the one-electron potential U applied to an OS depends on the contribution of the orbital from the OS to the band [27]. Therefore, if the contribution of the subspace of correlated orbitals to the band edges is small, the band-gap will remain almost unaffected. In the U=5 eV and U=10 eV schemes we have only applied the U to the d(Cu) orbitals of the transition metal atoms. We show later that the largest contribution to the VB edge is from d(Cu), p(S_1) and p(S_2) states, while that to the CB edge is from the p(M) states. This is the reason for using the U_a=5 eV and U_a=10 eV schemes. Note that these calculations are self-consistent and are not equivalent to the application of a scissor operator. This seems more reasonable

physically than applying a scissor operator or an artificial split in the bands ad hoc. This self-consistent corrections are limited by a *dilution* effect [27] because the changes induced by the self-interactions decrease with the mix between correlated orbitals with larger U and other orbitals with lower U (or U=0). This limits that a self-consistent DFT+U can be used extensively as a parametrized method for fit the energy band-gap or other properties. Of course it can be done with the application of a (non- self-consistent) scissor operator to the DFT results.

2. Projected density of states

M and S are V- and VI-group atoms respectively. The $CuMS_2$ materials are classified as low-valence Cu-V-VI compounds because that with the ionic model the V group atom has an oxidation state of +3. On the other hand, other Cu-V-VI compounds, such as Cu_3SbS_4, will be a high-valence Cu-V-VI compound (V^{5+}). Furthermore, other Cu-V-VI compounds such as the stoichiometric tetrahedrite $Cu_{12}Sb_4S_{13}$ would have a non-integer oxidation number of +3.5 according to the ionic model. In fact, the stoichiometric metallic tetrahedrite has the VB partially filled, i.e. with a metallic character[36]. In general, the tetrahedrites can be classified approximately as low-valence Cu-V-VI compounds. One of the main differences between the high-valence and low-valence Cu-V-VI compounds is the orbital contribution of V-group atoms to the band-gap edges. In the high/low-valence compounds the s(V)/p(V) orbital contribution to the CB is larger than that to the VB [13,36,37]. From our analyses of the projected density of states (PDOS) as a function of energy (Figure 2), the states of the VB edge are derived mainly from d(Cu), $p(S_1)$ and $p(S_2)$ states whereas the CB edge states are derived mainly from p(M) states, and with a lower contribution of the $p(S_1)$ and $p(S_2)$ states. These results are in agreement with Cu-V-VI ternary compound results in the literature [13,23,36,37].

3. Absorption coefficients

In addition to a suitable energy band-gap, a good candidate for photovoltaic applications must also have high optical absorption. We also calculate the absorption coefficient of $CuMS_2$ materials (Figure 3). For a better comparison, we shift the energy scale by the respective band-gap energies so that the onset to absorption occurs at zero energy. The main conclusion when GGA and GGA+U are compared is that the results remain qualitatively unchanged irrespective of the GGA+U scheme used. This occurs despite the different value for each GGA+U scheme of the single-particle energies, occupations and matrix elements of the momentum operator necessary for obtaining the absorption coefficients. The main quantitative changes are mainly in the energy band-gap.

In order to analyze the main contributions to the absorption coefficients, we are going to quantity the effect of the intra- and inter-atomic species transitions. The optical properties depend on the square of the momentum operator matrix elements. The momentum matrix elements $p_{\mu\lambda}$ between the μ and λ bands can be split into symmetrically non-equivalent chemical species contributions such as $p_{\mu\lambda} = \sum_A \sum_B p_{\mu\lambda}^{AB}$, where $p_{\mu\lambda}^{AA}$ is the intra-species component that couples the localized basis set functions on the same species atom A, and $p_{\mu\lambda}^{AB}$ is the inter-species component that couples the basis set functions on different species atoms A and B. Their square can be separated into three terms: intra-species (depending on $|p_{\mu\lambda}^{AA}|^2$) and inter-species (depending on $|p_{\mu\lambda}^{AB}|^2$ involving two species, and depending on $|p_{\mu\lambda}^{AB}||p_{\mu\lambda}^{CD}|$ involving three and four different species). Similarly, the absorption coefficients and other optical properties can be split. In Figure 4 we have represented the intra- and inter-species absorption coefficient components of the $CuMS_2$ materials with larger contribution. From the

figure, the largest contribution to the absorption coefficients around the energy band-gap, from larger to lower contributions, corresponds to M→M, S_1→S_1, S_2→S_2 and S_i-M (i=1,2) transitions.

From previous PDOS analyses, the largest contributions to the VB are from d(Cu), p(S_1) and p(S_2) states, and from p(M), p(S_1) and p(S_2) states to the CB. Then, it could be deduced that the high absorption arises from d(Cu) → p(M) and s(M) → p(M), and with a lower contribution from p(S_i)→p(S_j) (i,j=1,2) transitions because of the high joint DOS. However, in this simplified assumption we have not taken into account an essential element: the transition probabilities. Note that the optical properties will be proportional to the joint DOS if all the momentum operator matrix elements are equal. In order to clarify this aspect we have obtained the mean-value of $< p^2_{AB} >$ for all A→B transitions, i.e. $< p^2_{AB} >= \sum_{\mu<\lambda} \int d\vec{k} \cdot [f_{\mu,\vec{k}} - f_{\lambda,\vec{k}}] |p^{AB}_{\mu\lambda}|^2$. It is shown in Figure 5 scaled by the maximum value (M-M in Figure). From the Figure the largest value correspond to M→M transitions, and with lower proportion to S_1→S_1, S_2→S_2 and S_i-M transitions. The transition probabilities involving the Cu species are lower than the previous transitions. Therefore, the reason for the largest intra-species absorption coefficients of the M-M is their elevated transition probability. On the other hand, the low contribution of the intra- and inter-species absorption coefficients involving the Cu species is due to the low transition probabilities.

4. Efficiencies

In order to estimate the potentiality of $CuMS_2$ materials as solar-cell devices, we have obtained (Figure 6) the maximum efficiency for maximum solar concentration (f_c ~ 46200 suns, where 1 sun =1 KW/m^2) using several spectra. The efficiencies depend on the spectrum used and the spectral intensity (f_C =1 suns correspond to the spectrum

without concentration and $f_C^{(\max)} \sim$ 46200 suns correspond to maximum spectral intensity/concentration). The spectrum of a 5760 K black body reduced by the factor 46200 (BB) is usually used, because it has a simple analytic equation. Nevertheless, the same analysis can be done using other standard spectra[38]: extraterrestrial radiation (solar spectrum at top of the atmosphere) at mean Earth-Sun distance (AM0), spectral radiation from the solar disk plus sky diffuse and diffuse reflected from the ground on south facing surface tilted 37 deg from horizontal (AM1.5), Direct + Circumsolar spectrum (AM1.5D), etc. Of course, there are some improper spectra-concentration combinations. Nevertheless, it is used with a comparison objective as it is usual.

The efficiency of a solar cell can be calculated by using the ratio of the cell power output to the power cell density received. The models [39-41] used to obtain maximum efficiencies assume that any non-radiative recombination is suppressed, carrier mobilities are infinite (no ohmic losses), illumination comes from an isotropic gas of photons, and the cell absorbs all incident photons above the band-gap. The latter implicitly implies that the absorption coefficients are a step function (0 for $E < E_g$ and a constant for $E \geq E_g$, where E_g is the energy semiconductor band-gap). At the maximum concentration the maximum efficiency obtained using the BB spectrum is around 41% at E_g = 1.1 eV [39-41].

Under ideal conditions, a particle balance gives the net rate of current flow between bands corresponding to the electron transitions per unit illuminated area. The current flowing out of the device *J* must equal the difference between the number of photons absorbed and the number of photons emitted from the device due to radiative recombination:

$$J = J_{abs} - J_{emi} = q\left\{\left(\frac{f_C}{f_C^{(\max)}}\right)\int_0^\infty a(E,w)g_{abs}(E)dE - \int_0^\infty g_{emi}(E)dE\right\} \qquad (2)$$

where g_{abs} and g_{emi} are the absorbed and emitted photon flux densities, $a(E,w) \simeq 1 - e^{-\alpha(E)2w}$ is the absorptivity, α is the absorption coefficient, w is the device thickness, q is the electron charge, f_C is the light concentration factor ($1 \le f_C \le f_C^{(\max)}$ =46200). The first term on the right-hand side represents the sunlight absorbed by the solar cell, while the second term represents the light emitted by the solar cell due to radiative recombination.

Typically, it is assumed that both sun (at temperature T_S=5760 K) and ambient (at temperature $T_A \sim 300$ K) radiate like black bodies, producing isotropic photon fluxes described by the Plank distribution. In this case the photon flux densities are: $g_{abs} = g_{BB}(E,T_S,0) + (f_C^{(\max)} / f_C - 1) g_{BB}(E,T_A,0)$, and $g_{emi} = g_{BB}(E,T_A,\mu)$. Here $g_{BB}(E,T,\mu) = (2\pi / h^3 c^2) E^2 / [e^{(E-\mu)/kT} - 1]$ is the black body photon flux density, h is Planck's constant, c is the speed of light, k is the Boltzmann's constant, and $\mu = qV$ is the chemical potential associated with the emitted radiation, proportional to the applied bias V [39-41]. The first term of g_{abs} represents the sunlight coming directly from the sun which is absorbed by the solar cell, while the second term represents the sky radiation that is absorbed by the cell. Instead of the previous blackbody formulation it is possible to use models based upon measured data for the solar flux striking the surface of the earth [38]. In this case the tabulated solar flux g_{abs} must be used.

The output power density and the efficiency of the device are $P_{out} = VJ$ and $\eta = P_{out} / P_{abs}$ respectively, where P_{abs} is the absorbed power. They depend on the absorption coefficient, on the device thickness, on the current flow J and the applied bias V. To obtain the maximum efficiency with α and w fix it is needs to maximize η solving a non-linear equation because J depend on V. Furthermore, in order to achieve the maximum efficiency the cell should absorb all incident photons above the band-gap.

As has already been mentioned it implies the assumption of a step absorption coefficient (α=0 for $E < E_g$, and α=C for $E \geq E_g$, where C is a large constant). As a consequence the absorptivity is also a step function (a=0 for $E < E_g$, and a=1 for $E \geq E_g$), thus eliminating the dependence on w of P_{out} and η.

In order to calculate the $CuMS_2$ solar-cell device's maximum efficiencies we have assumed the usual approximation except that the cell absorbs all incident photons above the band-gap. The amount of light absorbed depends on the optical path length and the absorption coefficient. We have used the absorption coefficients obtained from first-principles instead of step functions. From previous discussions the absorption coefficient results are similar for the different GGA+U schemes when scaled by the respective band-gap energies. Despite the similarity, the band-gap is different. Therefore, the solar spectrum absorbed is different and the efficiencies depend on the GGA+U scheme. In order to obtain efficiencies we have chosen the scheme with the largest energy band-gap, i.e. closer to the experimental energy band-gaps. Because the absorption coefficients are not step functions, the efficiencies depend additionally on the thickness w of the device (Figure 6). From the figure, solar cell devices based on $CuMS_2$ materials with a few microns thick could reach efficiencies close to the maximum overall efficiency (~ 41%). It shows the huge potentiality of these materials as solar cell absorbers of the solar spectrum.

Further detailed analyses of the efficiencies, with light concentration and confinement techniques, and the current-voltage characteristics will be carried out in the near future. This would allow the thickness of the cell to be reduced without degrading the light absorption.

IV. CONCLUSIONS

We have analyzed the electronic, structural and optical properties of $CuMS_2$ (M=Sb, Bi) compounds using first-principles techniques in order to provide a more profound fundamental insight into these properties. In particular, the optical properties are of direct relevance to the use of these materials as solar radiation absorbers in solar cells. The results have been compared with other (theoretical and experimental) data in the literature, which agree well with the available data. In particular, comparison with the experimental absorption coefficients is good. The comparison with the experimental optical properties is more demanding than the energies and band structure comparisons. It is because of the optical properties involve, in addition to the electronic structure, the occupations and the transition probabilities.

Furthermore, both the electronic and optical properties have been split into atomic, orbital, and inter- and intra-(symmetrically non-equivalent) species contributions in order to understand microscopically the high light absorption of these materials, about twice as large as in the conventional Cu-based photovoltaic materials. From these analyses, the elevated absorption in these materials is because of the larger M-M, S_1-S_1, and S_2-S_2 intra-specie optical transitions.

Finally, the potentiality of $CuMS_2$ materials as solar-cell devices have been analyzed by obtaining the maximum efficiency for maximum solar concentration using the optical absorption coefficients obtained previously from our first-principles calculations. The results indicate that with small-width devices efficiencies near to the maximum overall theoretical limit could be achieved.

Acknowledgments

This work has been supported by the National Spanish projects PROMESA (ENE2012-37804-C02-01) and MADRID-PV (S2013/MAE-2780).

References

[1] J. Britt and C. Ferekides, Thin-film CdS/CdTe Solar Cell with 15.8% Efficiency. *Appl. Phys. Lett.* **1993***, 62*, 2851-2852.

[2] S. Siebentritt, M. Igalson, C. Persson, and S. Lany, The Electronic Structure of Chalcopyrites- Bands, Point Defects and Grain Boundaries. *Prog. Photovoltaics* **2010***, 18*, 390-410.

[3] C. Tablero and D. Fuertes Marrón. Analysis of the Electronic Structure of Modified $CuGaS_2$ with Selected Substitutional Impurities: Prospects for Intermediate Band Thin Film Solar Cells Based on Cu-containing Chalcopyrites. *J. Phys. Chem. C* **2010***, 114*, 2756-2763.

[4] C. Tablero. Electronic and Optical Properties of the Group IV Doped Copper Gallium Chalcopyrites. *Thin Solid Films* **2010***, 519*, 1435–1440.

[5] C. Tablero. Ionization Levels of Doped Copper Indium Sulfide Chalcopyrites. *J. Phys. Chem. A* **2012***, 116*, 1390-1395.

[6] C. Tablero, Effect of the Oxygen Isoelectronic Substitution in Cu_2ZnSnS_4 and their Photovoltaic Application. *Thin Solid Films* **2012***, 520*, 5011–5013.

[7] C. Tablero. Electronic and Photon Absorber Properties of Cr-Doped Cu_2ZnSnS_4. *J. Phys. Chem. C* **2012***,* 116, 23224–23230.

[8] C. Tablero. Ionization Energies of Amphoteric-doped Cu_2ZnSnS_4: Photovoltaic Application. *J. Alloys Compd.* **2014***, 586*, 22–27.

[9] C. Tablero. Electronic and Optical Properties of Substitutional V, Cr and Ir Impurities in Cu_2ZnSnS_4. *Sol.Ener.Mat.Sol.C.* **2014***, 125*, 8–13.

[10] H. Katagiri, Cu_2ZnSnS_4 Thin Film Solar Cells *Thin Solid Films* **2005***, 480-481*, 426-432.

[11] T. K. Todorov, K. B. Reuter, and D. B. Mitzi, High-Efficiency Solar Cell with Earth-Abundant Liquid-Processed Absorber. *Adv. Mater.* **2010***, 22*, E156-E159.

[12] J. Zhou, G.-Q. Bian, Q.-Y. Zhu, Y. Zhang, C.-Y. Li, J. Dai, Solvothermal Crystal Growth of $CuSbQ_2$ (*Q*=S, Se) and the Correlation Between Macroscopic Morphology and Microscopic Structure, *Journal of Solid State Chemistry* **2009***, 182*, 259-264.

[13] L. Yu, R. S. Kokenyesi, D. A. Keszler and A. Zunger, Inverse Design of High Absorption Thin-Film Photovoltaic Materials, *Adv. Energy Mater.* **2013***, 3*, 43–48.

[14] Y. Rodríguez-Lazcano, M.T.S. Nair, P.K. Nair, $CuSbS_2$ Thin Film Formed Through Annealing Chemically Deposited Sb_2S_3–CuS Thin Films, *J. Cryst. Growth* **2001***, 223*, 399-406.

[15] A. Rabhi, M. Kanzari, and B. Rezig, Optical and structural properties of $CuSbS_2$ Thin Films Grown by Thermal Evaporation Method. *Thin Solid Films* **2009***, 517*, 2477-2480.

[16] S. H. Pawar, A. J. Pawar, and P. N. Bhosale, Spray Pyrolytic Deposition of $CuBiS_2$ Thin Films. *Bull. Mater. Sci.* **1986***, 8*, 423-426.

[17] P. S. Sonawane, P. A. Wani, L. A. Patil, and T. Seth, Growth of $CuBiS_2$ Thin Films by Chemical Bath Deposition Technique from an Acidic Bath. *Mater. Chem. Phys.* **2004***, 84*, 221-227.

[18] M. Kumar and C. Persson, $CuSbS_2$ and $CuBiS_2$ as Potential Absorber Materials for Thin-Film Solar Cells. *J. Renewable Sustainable Energy* **2013***, 5*, 031616 1-6.

[19] S. Manolache, A. Duta, L. Isac, M. Nanu, A. Goossens, J. Schoonman, The Influence of the Precursor Concentration on $CuSbS_2$ Thin Films Deposited from Aqueous Solutions. *Thin Solid Films* **2007***, 515*, 5957-5960.

[20] A. Rabhi, M. Kanzari, B. Rezig, Optical and Structural Properties of $CuSbS_2$ Thin Films Grown by Thermal Evaporation Method. *Thin Solid Films* **2009***, 517*, 2477-2480;

Rabhi, M. Kanzari, B. Rezig, Growth and Vacuum Post-annealing Effect on the Properties of the New Absorber $CuSbS_2$. Thin Films, *Matter. Lett.* **2008***, 62*, 3576–3578.

[21] Y. Rodríguez-Lazcano, M.T.S. Nair, P.K. Nair, $CuSbS_2$ Thin Film Formed Through Annealing Chemically Deposited Sb_2S_3–CuS Thin Films. *Journal of Crystal Growth* **2001***, 223*, 399-406.

[22] Y. Rodríguez-Lazcano, M.T.S. Nair, P.K. Nair, $Cu_xSb_yS_z$ Thin Films Produced by annealing Chemically Deposited Sb_2S_3-CuS Thin Films, *Mod Phys Lett B* **2001***,15*, 667.

[23] J. T. R. Dufton, A. Walsh, P. M. Panchmatia, L. M. Peter, D. Colombara and M. Saiful Islam, Structural and Electronic Properties of $CuSbS_2$ and $CuBiS_2$: Potential Absorber Materials for Thin-Film Solar Cells. *Phys. Chem. Chem. Phys.,* **2012***, 14*, 7229–7233.

[24] W. Kohn and L. J. Sham, Self-Consistent Equations Including Exchange and Correlation Effects, *Phys. Rev.* **1965***, 140*, A1133-A1138.

[25] J. M. Soler, E. Artacho, J. D. Gale, A. García, J. Junquera, P. Ordejon, and D. Sánchez-Portal, The SIESTA Method for Ab initio Order-N Materials Simulation, *J. Phys.: Condens. Matter* **2002***, 14,* 2745-2779, and references therein.

[26] V. I. Anisimov, J. Zaanen, and O. K. Andersen, Band Theory and Mott Insulators: Hubbard U instead of Stoner I, *Phys. Rev. B* **1991***, 44*, 943-954; V. I. Anisimov, I. V. Solovyev, and M. A. Korotin, M. T. Czyyk, and G. A. Sawatzky, Density-Functional Theory and NiO Photoemission Spectra, *Phys. Rev. B* **1993***, 48*, 16929–16934.

[27] C. Tablero, Representations of the Occupation Number Matrix on the LDA/GGA+U Method, *J. Phys.: Condens. Matter* **2008***, 20*, 325205 1-12.

[28] C. Tablero, Effects of the Orbital Self-interaction in both Strongly and Weakly Correlated Systems, *J. Chem. Phys.* **2009***, 130*, 054903 1-9.

[29] D. D. O'Regan, M. C. Payne, and A. A. Mostofi, Subspace Representations in Ab initio Methods for Strongly Correlated Systems, *Phys. Rev. B* **2011***, 83*, 245124 1-14.

[30] M. Grisolía, P. Rozier, and M. Benoit, Density Functional Theory Investigations of the Structural and Electronic Properties of $Ag_2V_4O_{11}$, *Phys. Rev. B* **2011***, 83*, 165111 1-12.

[31] J. P. Perdew, K. Burke, and M. Ernzerhof, Generalized Gradient Approximation Made Simple, *Phys. Rev. Lett.* **1996***, 77*, 3865-3868.

[32] N. Troullier and J. L. Martins, Efficient Pseudopotentials for Plane-wave Calculations, *Phys. Rev. B* **1991***, 43*, 1993-2003.

[33] L. Kleinman and D. M. Bylander, Efficacious Form for Model Pseudopotentials, *Phys. Rev. Lett.* **1982***, 48*, 1425-1428; D. M. Bylander and L. Kleinman, 4f Resonances with Norm-conserving Pseudopotentials, *Phys. Rev. B* **1990***, 41*, 907-912.

[34] O. F. Sankey and D. J. Niklewski, Ab initio Multicenter Tight-binding Model for Molecular-dynamics Simulations and Other Applications in Covalent Systems, *Phys. Rev. B* **1989***, 40*, 3979-3995.

[35] M. F. Razmara, C. M. B Henderson, R. A. D. Pattrick, The Crystal Chemistry of the Solid Solution Series between Chalcostibite ($CuSbS_2$) and Emplectite ($CuBiS_2$). *Mineralogical Magazine* **1997***, 61*, 79-88.

[36] C. Tablero, Electronic and Optical Property Analysis of the Cu−Sb−S Tetrahedrites for High-Efficiency Absorption Devices, *J. Phys. Chem. C* **2014***, 118*, 15122-15127.

[37] T. Shi, W-J Yin, M. Al-Jassim and Y. Yan, Structural, Electronic, and Optical Properties of Cu_3-V-VI_4 Compound Semiconductors. *Appl. Phys. Lett.* **2013***, 103*, 152105 1-4.

[38] ASTM G173-03 Reference Spectra:
http://rredc.nrel.gov/solar/spectra/am1.5/ASTMG173/ASTMG173.html

[39] A. Luque and A. Martí, Theoretical Limits of Photovoltaic Conversion, in Handbook of Photovoltaic Science and Engineering Edited by A. Luque and S. Hegedus, John Wiley & Sons Ltd (**2003**).

[40] P. Würfel, Physics of Solar Cells. From Principles to New Concepts, **2005** WILEY-VCH Verlag GmbH & Co, KGaA.

[41] M.A. Green, Third Generation Photovoltaics. Advanced Solar Energy Conversion, Springer-Verlag Berlin Heidelberg **2003, 2006**.

List of Figures

Figure 1: $CuMS_2$ energy-band diagram for (a) M=Sb and (b) M=Bi. The VB edge energy has been chosen as the origin of the energy.

Figure 2: Projected DOS on species states with more contribution to the VB and the CB edges for the (a) chalcostibite (M=Sb) and (b) emplectite (M=Bi). The VB edge has been chosen as the origin of the energy.

Figure 3: Absorption coefficients α(E) with several U schemes (see text) for the (a) chalcostibite (M=Sb) and (b) emplectite (M=Bi). The large points correspond to experimental data in [13] ('E1' label), and theoretical data in references [13] ('T1' label) and [18] ('T2' label). The energy scale has been shifted by the respective band-gap energies so that onset to absorption occurs at zero energy.

Figure 4: Intra-(symmetrically non-equivalent) species $CuMS_2$ absorption coefficient components of the (a) chalcostibite (M=Sb) and (b) emplectite (M=Bi). The respective band-gap energies have been chosen as the origin of the energy.

Figure 5: Mean-value of the p_{AB}^2 for all A→B transitions scaled by the maximum value.

Figure 6: Efficiency η (%) as a function of the cell thickness w with several standard spectra, and for maximum concentration (f_C ~ 46200 suns, sun units=1 Kw/m^2). The marks indicate the calculated values. Lines between the marks have been added for visual effect.

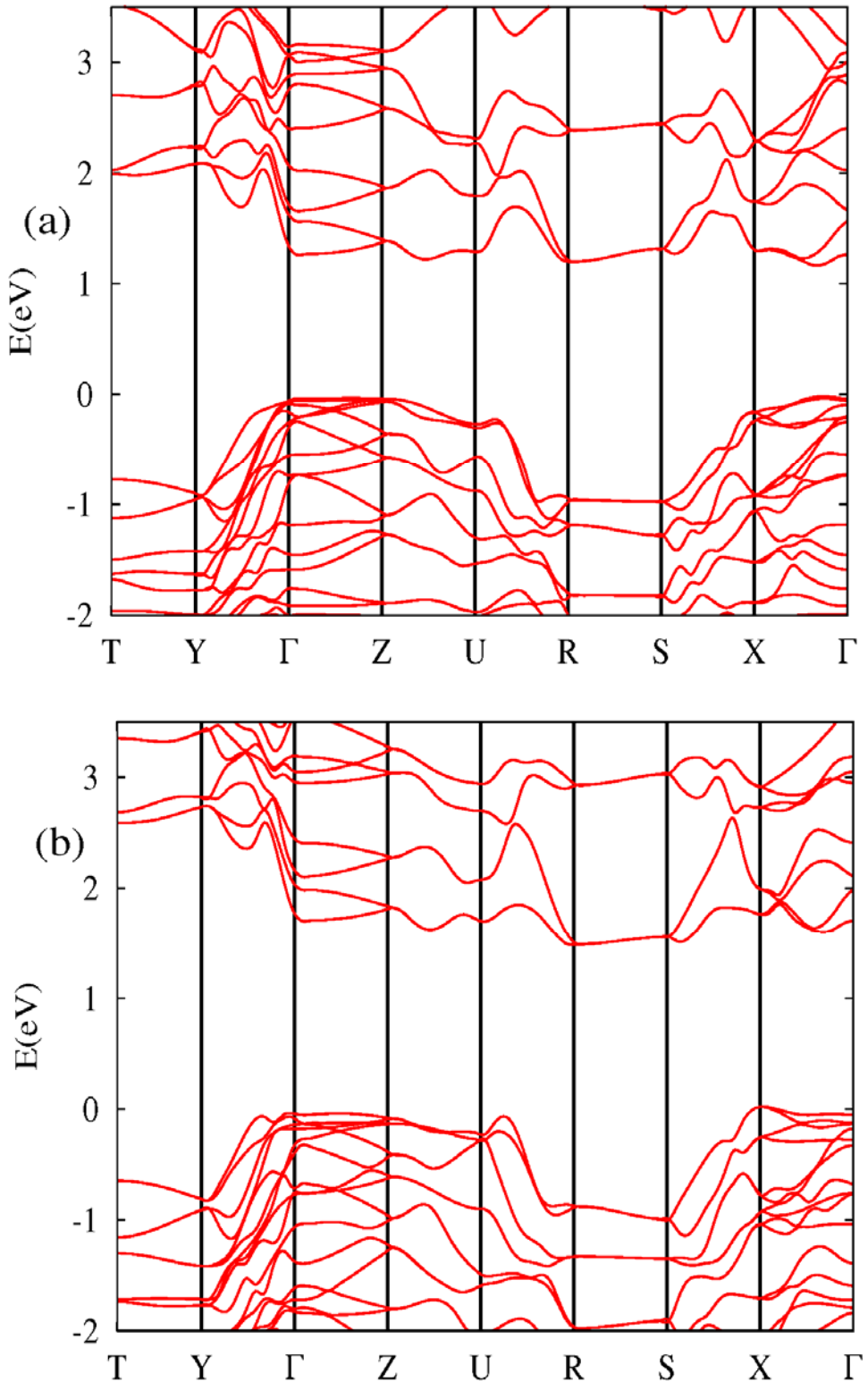

Figure 1

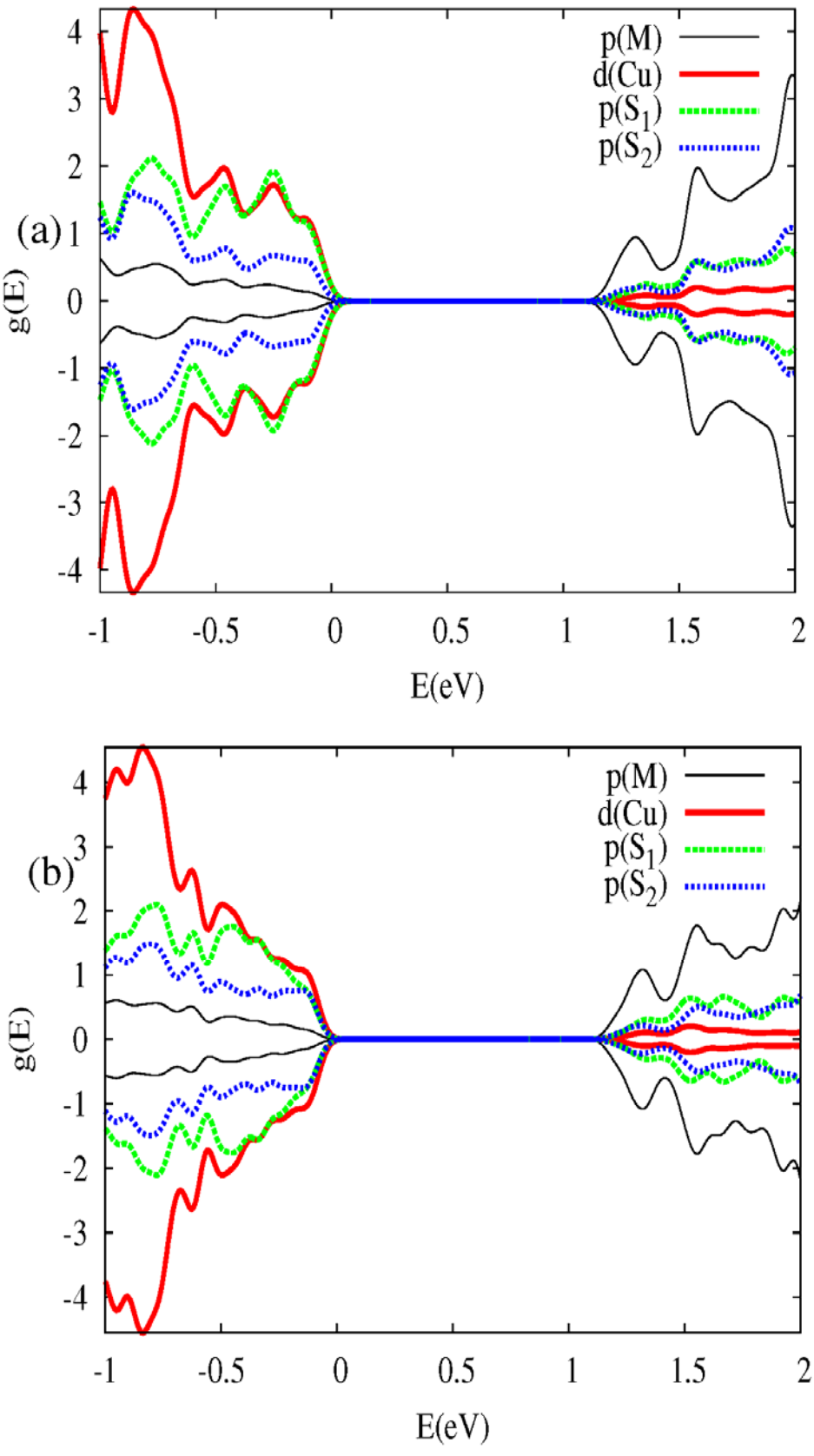

Figure 2

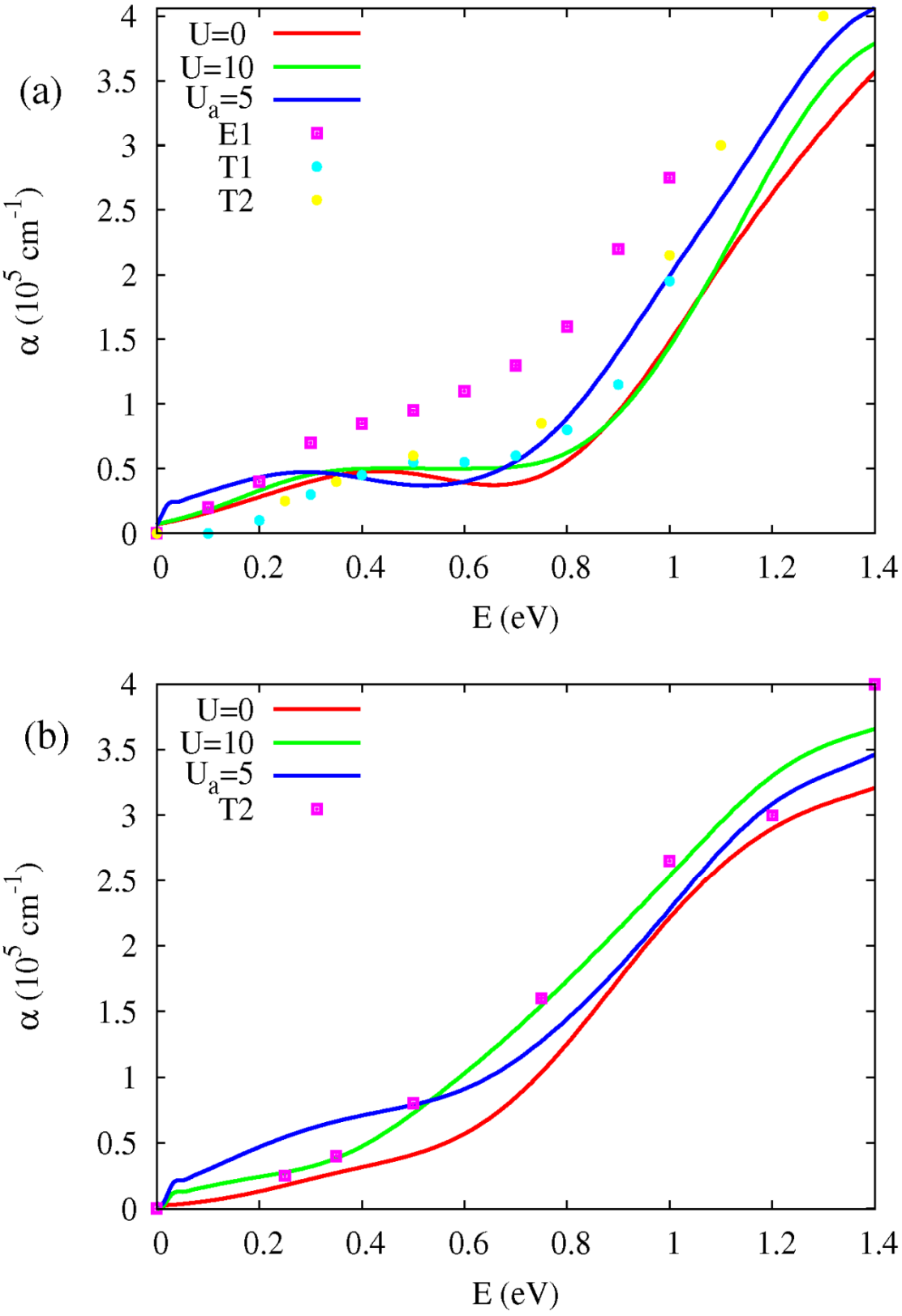

Figure 3

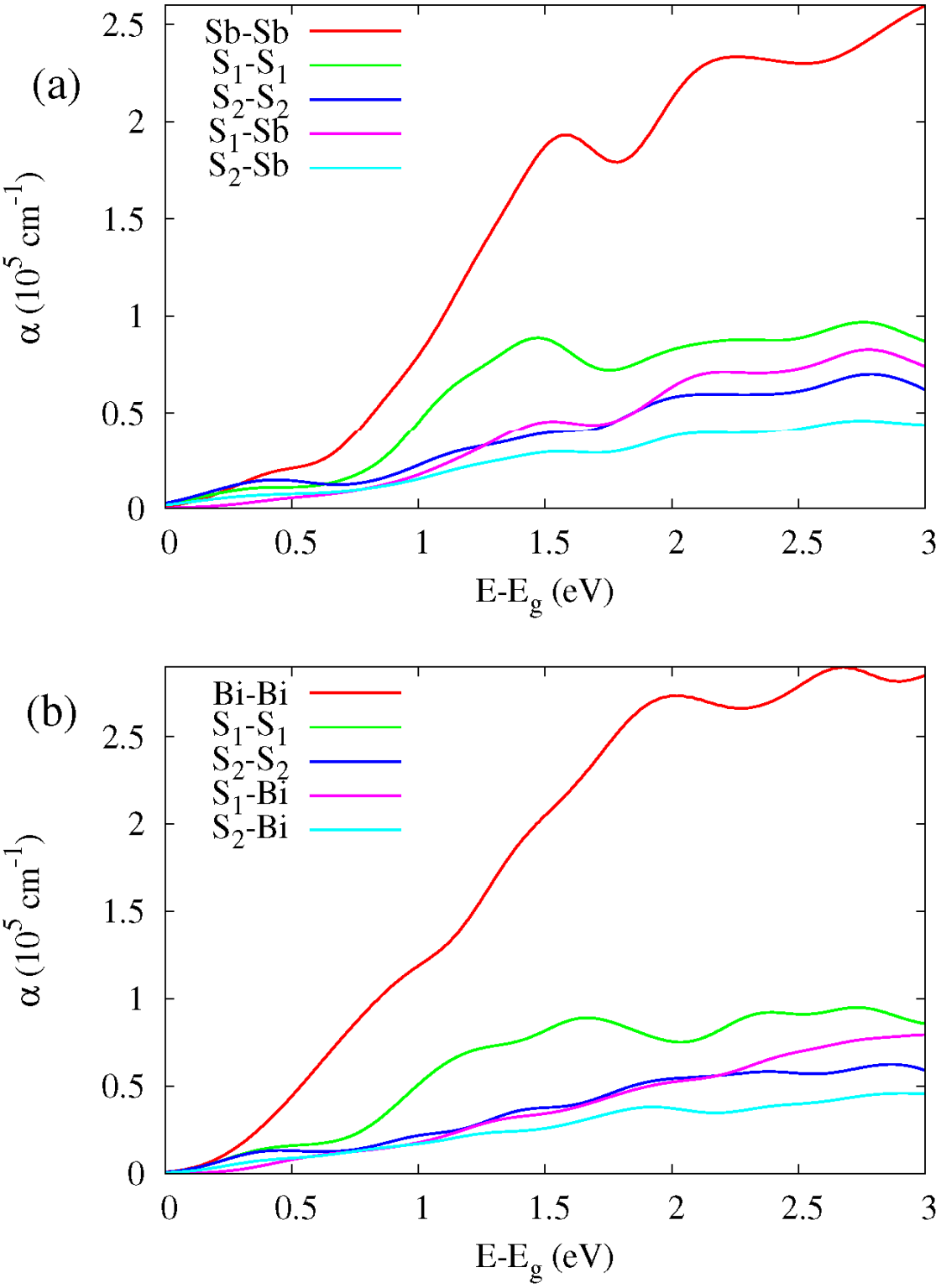
(a)
Sb-Sb
S1-S1
S2-S2
S1-Sb
S2-Sb
α (10^5 cm^-1)
E-Eg (eV)
(b)
Bi-Bi
S1-S1
S2-S2
S1-Bi
S2-Bi
α (10^5 cm^-1)
E-Eg (eV)

Figure 4

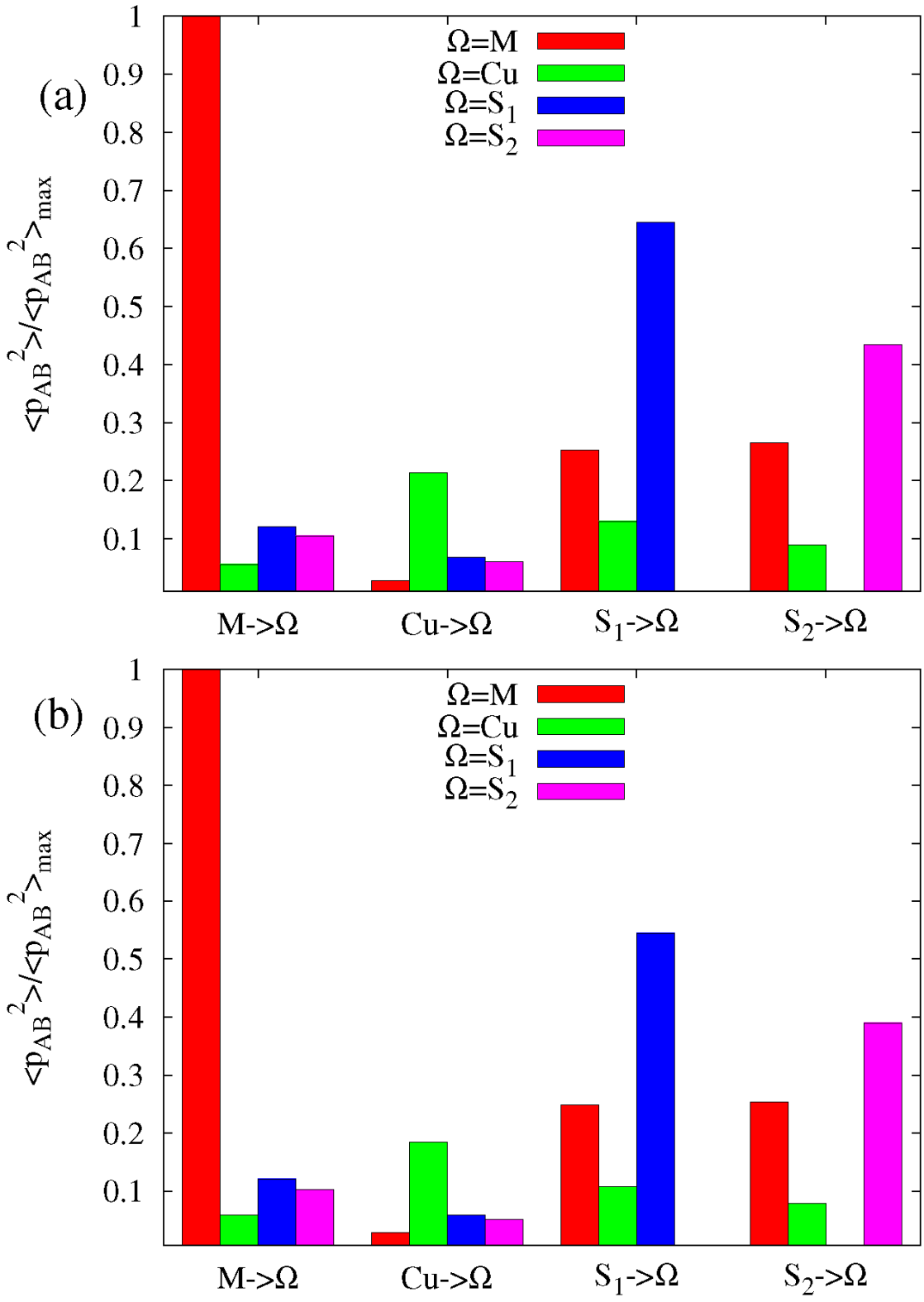
(a)
(b)
Ω=M
Ω=Cu
Ω=S1
Ω=S2
<pAB2>/<pAB2>max
1
0.9
0.8
0.7
0.6
0.5
0.4
0.3
0.2
0.1
M->Ω
Cu->Ω
S1->Ω
S2->Ω

Figure 5

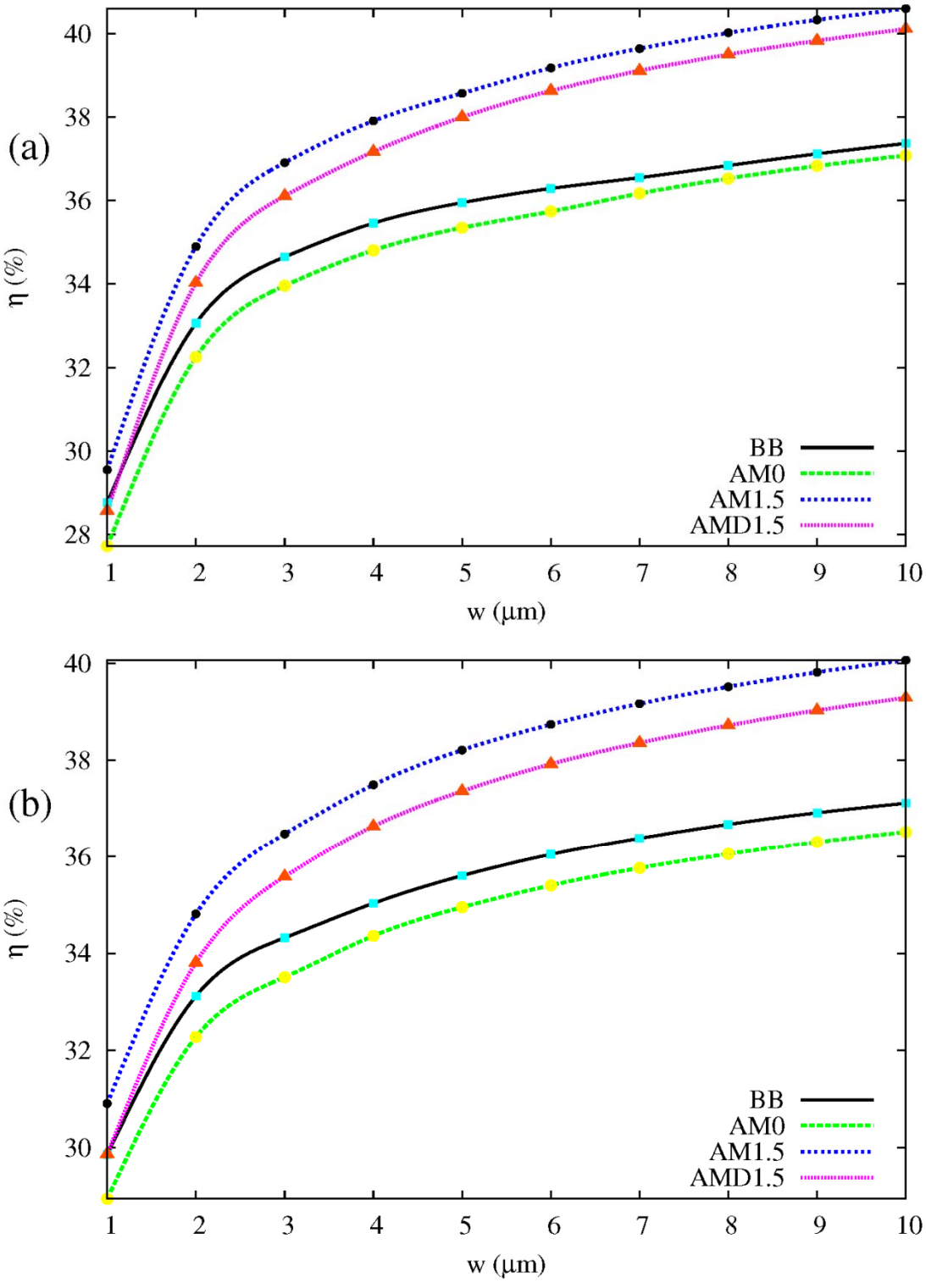

Figure 6

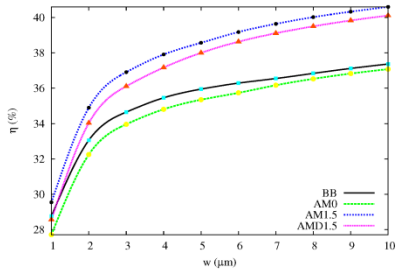

For Table of Contents Only